*Article*

# Aging Triggers H3K27 Trimethylation Hoarding in the Chromatin of Nothobranchius Furzeri Skeletal Muscle

**Chiara Cencioni [1,#], Johanna Heid [2,#], Anna Krepelova [3], Seyed Mohammad Mahdi Rasa [3], Carsten Kuenne [4], Stefan Guenther [4], Mario Baumgart [3], Alessandro Cellerino [5], Francesco Neri [3], Francesco Spallotta [6,*] and Carlo Gaetano [7,*]**

[1] National Research Council, Institute of Cell Biology and Neurobiology (IBCN), Rome, 00143, Italy; chcencioni@gmail.com

[2] Division of Cardiovascular Epigenetics, Department of Cardiology, Goethe University, Frankfurt am Main, 60596, Germany; johannaheid@yahoo.de

[3] Leibniz Institute on Aging - Fritz Lipmann Institute (FLI), Jena, 07745, Germany; (A.K.) Anna.Krepelova@leibniz-fli.de; (S.M.M.R.) Mahdi.Rasa@leibniz-fli.de; (M.B.) Mario.Baumgart@leibniz-fli.de; (F.N.) francesco.neri@leibniz-fli.de

[4] ECCPS Bioinformatics and deep sequencing platform, Max Planck Institute for Heart and Lung Research, Bad Nauheim, 61231, Germany; (C.K.) carsten.kuenne@mpi-bn.mpg.de; (S.G.) Stefan.Guenther@mpi-bn.mpg.de

[5] Scuola Normale Superiore, Laboratory of Biology (Bio@SNS), c/o Istituto di Biofisica del CNR, Pisa, 56124, Italy; alessandro.cellerino@gmail.com

[6] Cancer Epigenetics Laboratory, Department of Oncology, University of Turin, c/o Candiolo Cancer Institute FPO-IRCCS, Candiolo (Turin), 10060, Italy; francesco.spallotta@unito.it

[7] Laboratory of Epigenetics, Istituti Clinici Scientifici Maugeri IRCCS, 27100 Pavia, Italy; carlo.gaetano@icsmaugeri.it.

* Correspondence:
Francesco Spallotta, PhD
Cancer Epigenetics Laboratory, Department of Oncology, University of Turin, c/o Candiolo Cancer Institute FPO-IRCCS, km 3,95, SP142, 10060, Candiolo (Turin), Italy; e-mail: francesco.spallotta@unito.it; Ph. +39 011 993 3523. (F.S.)
Carlo Gaetano, MD
Laboratorio di Epigenetica, Istituti Clinici Scientifici Maugeri, Via Maugeri 4, Pavia, Italy; e-mail: carlo.gaetano@icsmaugeri.it; Ph. +39 0382592262 (C.G.)

# CC and JH co-first authors.

* FS and CG co-senior authors.

**Abstract:** Aging associates with progressive loss of skeletal muscle function leading up to sarcopenia, a process characterized by impaired mobility and weakening of muscle strength. Molecular mechanisms underpinning sarcopenia are still poorly characterized. Since aging associates with profound epigenetic changes, epigenetic landscape alteration analysis in the skeletal muscle promises to highlight molecular mechanisms of age-associated sarcopenia. The study was conducted exploiting the short-lived turquoise killifish *Nothobranchius furzeri* (*Nfu*), a relatively new model for aging studies. The epigenetic analysis suggested for a less accessible and more condensed chromatin in old *Nfu* skeletal muscle. Specifically, an accumulation of heterochromatin regions was observed as consequence of increased levels of H3K27me3, HP1α, polycomb complex subunits and senescence associated heterochromatic foci (SAHFs). Consistently, euchromatin histone marks, including H3K9ac, decreased. The integrative bioinformatics analysis of RNASeq and ChIPSeq, related to skeletal muscle of *Nfu* at different ages, revealed a down-modulation of genes involved in cell cycle, differentiation and DNA repair and an up-regulation of inflammation and senescence genes. Undoubtedly, more studies are needed to disclose the detailed mechanisms, but this approach revealed an unprecedented specific features of *Nfu* skeletal muscle aging, potentially

associated with sarcopenia onset and consequent impairment of swimming and mobility typical of old *Nfu*.

**Keywords:** aging; skeletal muscle; sarcopenia; frailty; chromatin; epigenetic changes; histone modifications; Nothobranchius furzeri

## 1. Introduction

In the last two centuries, Western Country life expectancy considerably increased dramatically enlarging the elderly people population. Consequently, the cost of healthcare raised significantly in association with the multimorbidity and chronicity that characterize elderly patients [1-3]. By 2050 more than one fifth of the global population will be older than 60 years and about 5% will be over 80 [1-3]. Accordingly, the risk to develop aging-associated diseases, including cardiovascular diseases, dementias and cancers, will continue to rise [4], significantly challenging worldwide health and social systems. Aging is accompanied by an overall loss of fitness and a decline of cell and organ function, associated with a reduced regenerative capacity and life expectancy [5]. In this context, the understanding of aging associated molecular mechanisms is an unmet need to test novel approaches able to promote healthy aging and improve life quality in the growing elderly population.

Among the common features of aging, elderly people experiences loss of muscle mass, a phenomenon known as sarcopenia, associated with frailty, impaired health span and reduced quality of life [6]. Indeed, sarcopenia is present in over 40% of people older than 60 years with weaken muscle strength and impaired physical activity and movement [6]. Of note, sarcopenia contributes to the onset of different age-associated diseases and develops mostly as consequence of chronic inflammation and mitochondrial dysfunction [7,8], two common alterations associated with aging paralleled by loss of proper protein synthesis, metabolic pathway switch and neuronal signaling alteration [8]. The reduction of muscle mass typical of elderly people derived also from an impairment in the regenerative capacity after injury caused by an exhaustion of the muscle stem cell pools consisted of satellite cells [6]. Although sarcopenia is a common feature of aging [9], the underpinning molecular mechanisms involved in the onset have been poorly characterized and, at moment, the only effective prevention is represented by an extensive lifestyle change aimed to balance physical workout and diet [8].

Physiologically, the aging process associates with profound epigenetic changes, which broadly affect the genome architecture and the epigenetic landscape, ultimately altering gene expression [2,3]. Epigenome control relies on DNA methylation, histone-modifying complexes and non-coding RNA activity [10]. Importantly, DNA methylation plays an important mechanistic role in aging [11], being few hundred specific CpG site methylation changes, either hypermethylated or hypomethylated, predictive of biological age in a variety of species including rodents, primates and humans [12]. DNA methylation usually harbors specific methylated histone residues, including histone 3 (H3), lysine (K) 27, and lysine 9 tri-methylation (H3K27me3; H3K9me3) [13], which contribute to the establishment of heterochromatic regions within the genome. Indeed, H3K27me3 and H3K9me3 enriched regions are characterized by the formation of senescence-associated heterochromatin foci (SAHFs) [14], nuclear DNA domains densely stained by DAPI, associated with distinct heterochromatin structures in stress-induced senescent cells characterized by cell growth arrest and transcription repression [15]. SAHFs actively contribute to the interruption of cell proliferation by repression of the cell cycle activator transcription factor E2F [16]. On the contrary, acetylation of histones is rather associated with an open chromatin configuration, transcript elongation and therefore an active gene expression [17]. Open chromatin is characterized by regions enriched in histone 4 (H4), K 16 and H3K9 acetylation (ac) (H4K16ac; H3K9ac) [18,19]. During aging histone modifications change and affect gene expression, genomic stability, DNA repair and replication [2,5]. In humans, global DNA and histone methylation is decreased with age, but it might be accumulated at specific loci [20], leading to a loss of heterochromatin and increasing genome instability, which favor DNA damage, inflammation and disease development [21]. Alteration in histone modifications also depends on the

functional deregulation of histone methylase complexes, like the polycomb repressive complex member EZH2 (PRC2) and Bmi1 (PRC1) as well as the histone demethylase jumonji domain containing 3 (JMJD3) [22].

In the present study, we investigated the epigenetic landscape of young (5 weeks old), adult (12-21 weeks old) and old (27-40 weeks old) *Nothobranchius furzeri* (*Nfu*) skeletal muscle tissue to gain insights about epigenetic changes associated with aging and the related impact on chromatin structure and cellular transcriptome. In recent years, the turquoise killifish *Nfu* has been established as a model for aging research [23-25] due to its exceptional short lifespan (3-9 months) [26] and its capacity to resemble many hallmarks of mammalian aging [27,28] such as sarcopenia [29]. Indeed, old *Nfu* presents reduced locomotor activity as consequence of age-associated changes in skeletal muscle tissue [30]. The understanding of the aging-dependent epigenetic alterations might open the avenue for novel treatments aimed to promote healthy ageing possibly counteracting muscle fiber loss and the onset of sarcopenia.

## 2. Materials and Methods

### *2.1 In vivo experiments*

Whole skeletal muscle tissues were collected from male *Nfu* (strain MZM-04/10). *Nfu* samples were derived from fish at different ages: young (5 weeks), adult (12-21 weeks) and old (27-40 weeks). To avoid effects of circadian rhythms and feeding, animals were always sacrificed at 10 a.m. in fasted state. Tissue collection was performed in fishes euthanized with MS-222 and cooled on crushed ice. Then, RNA was extracted from tissues in a solution of cooled QIAzol (Qiagen) together with a 5 mm stainless steel bead (Qiagen). Homogenization was performed by TissueLyzer II (Qiagen). Proteins and DNA were extracted from flash frozen fish samples. Immunofluorescence was performed in paraformaldehyde (PFA) fixed tissue embedded in paraffin.

### *2.2 Cells and treatments*

Cells were isolated from *Nfu* skeletal muscle tissue minced on ice in PBS. Tissues from up to three individuals were pooled. Collagenase solution (1 mg/ml) was added to samples and incubated for 30 min on a rotation platform at 37° C. Then, digestion step was stopped, cell suspension was filtered and pellet was obtained by centrifugation at 350 g for 10 min at room temperature. To reduce contamination from fibroblasts, two pre-plating steps were performed. Thereafter, cells were plated in collagen-coated 6-well plates and incubated at 28° C. Cells were cultured in DMEM medium supplemented with 10% water, 20% FBS, 1% Penicillin/Streptomycin, 0,1 % Amphotericin and 0,05% Gentamycin. Medium was changed every other day and cells were split before reaching 80-90% of confluence.

### *2.3 Quantification of global DNA methylation*

DNA was extracted using the E.Z.N.A. DNA tissue kit (VWR OMEGA biotek) according manufacture's instruction. MethylFlash Methylated (5mC) DNA Quantification Kit was used to quantify methylation levels of DNA from fish and cellular samples according manufacturer's instruction (Epigentek). The optical density (OD) was detected by EnSpire Multimode Plate Reader (Perkin Elmer).

### *2.4 RNA extraction and qRT-PCR.*

RNA was extracted from *Nfu* tissue and cell samples using Tri-Reagent (Sigma-Aldrich) according to manufacturer's instruction. cDNA synthesis for quantitative real-time PCR (qRT-PCR) was carried out with SuperScript III First-Strand Synthesis Super Mix for qRT-PCR (Invitrogen) according to the manufacturer's protocol. All reactions were performed in 96-well format in the StepOne Plus Real-Time PCR System (Applied Biosystems) using ORA qPCR Green ROX H Mix (HighQu). For each gene of interest, qRT-PCR was performed as follows: each RNA sample was

tested in duplicate and insulin receptor a (ira) was used to normalize transcript abundance in *Nfu*. mRNA expression levels were calculated by Comparative Ct Method (Pfaffl, 2004) by using the Applied Biosystem software (Applied Biosystem) and were presented as fold induction of transcripts for target genes. Fold change above 1 denotes up-regulated expression, and fold change below 1 denotes down-regulated expression versus reference sample.

Primers sequences (Table 1) were selected using the primer3 software (Untergasser et al., 2012) based on published sequence data from NFINgb (http://nfingb.leibniz-fli.de/main.html?data=data/json/notho4) [31] and the Killifish Genome Browser (http://africanturquoisekillifishbrowser.org/) [32]. All primers were synthesized by Sigma-Aldrich.

**Table 1.** List of forward and reverse primers.

| Gene | Forward 5' - 3' | Reverse 5' - 3' |
|---|---|---|
| cbx2 | TCCCAACGGACAAAAGAAAC | TTGTTGGGTTTGGTGGATTT |
| cbx7.1 | GAGCAAGTGTTTGCTGTGGA | CTTTGGCACCTTTCTTCCTG |
| cbx7.2 | GGAGACAGGCTGGATTTTGA | GCCATGGTAACCGACTGATT |
| cbx8a | CAGTCAATCGGGGTGAAAGT | TTAGACTCCTCCGGGAACCT |
| cbx8b | AGGTGGCGAGTATCTGCTGT | CGGTTCCCAAGTGCTGTATT |
| cyclinb | GGTGGGAGACTTTGCCTACA | AGAGGGTCAGCTCCATCAGA |
| cyclind | CTGTGAGCTTTGCTGCTTTG | ACGCTCAGCAAACACATACG |
| eed | AGTCCTGTGAAAACGCCATC | AACGTAAAGCTTCCCCACCT |
| ezh1 | CAAGAGGATTCCCAGCGATA | GGGTTGGAGGAAACAGTCGTA |
| ezh2 | ATTCTGTCAACCCCAACTGC | ATGCCCACGTACTTCAGAGC |
| gadd45γ | ATTGCGCTTCAGATCCACTT | CGCAGAACAGACTCAGCTTG |
| ira | TGCCTCTTCAAACCCTGAGT | AGGATGGCGATCTTATCACG |
| kdm6a | GTCAAACCCTACCCCCTCAT | TGTGGAGAGAGGAGCCAACT |
| kdm6b | CAAAGCCAGCTTTCTGGAAC | TCTGGATGTGAGGAGCACAG |
| myog | GTTCGACCAAGCTGGCTATC | CATGGTCACCGTCTTCCTTT |
| p21 | CCCTGCGTAAAGATCTGGAG | ACCACCACCCTTCCTCTTT |
| pcna | ACCCTCAGAGCAGAGGACAA | CATGGGAAAGGATCTGGAAA |
| polγ | TCCCCGTTAATCAGAACTGG | TCTGCTGCTTTTTGGGAGTT |
| ssbp1 | CTGGAGAGACGGAAACAAGC | CTGACGTTGTCGCTCAGAAA |
| suz12 | AAAGGAGCAAAGGTGGAGGT | GACGGTTGTGACCACTGATG |
| tfam | TACGTGTCCGAGCACTTTCA | CATGTGGTCTTCCCAGGACT |

*2.5 Sequencing and bioinformatics analysis*

For RNA sequencing, RNA was isolated from skeletal muscle tissue from 3 fishes for each condition (young, adult and old) using the miRNeasy micro Kit (Qiagen) combined with on-column DNase digestion (DNase-Free DNase Set, Qiagen) to avoid contamination by genomic DNA. RNA and libraries integrity were verified with LabChip Gx Touch 24 (Perkin Elmer). 1µg of total RNA was used as input for SMARTer Stranded Total RNA Sample Prep Kit - HI Mammalian (Clontech). Sequencing was performed on the NextSeq500 instrument (Illumina) using v2 chemistry, resulting in average of 30M reads per library with 2x75bp paired end setup. The resulting raw reads were assessed for quality, adapter content and duplication rates with FastQC (Available online at http://www.bioinformatics.babraham.ac.uk/projects/fastqc). Trimmomatic version 0.33 was employed to trim reads after a quality drop below a mean of Q20 in a window of 5 nucleotides. Only reads above 30 nucleotides were cleared for further analyses. Trimmed and filtered reads were aligned versus the *Nothobranchius furzeri* genome version NotFur1 using STAR 2.4.2a with the parameter "--outFilterMismatchNoverLmax 0.1" to increase the maximum ratio of mismatches to mapped length to 10%. The number of reads aligning to genes was counted with featureCounts 1.4.5-p1 tool from the Subread package. Only reads mapping at least partially inside exons were admitted and aggregated per gene. Reads overlapping multiple genes or aligning to multiple regions were excluded. Differentially expressed genes were identified using DESeq2 version 1.62.25. Only genes with a minimum fold change of +- 2, a maximum Benjamini-Hochberg corrected p-value of 0.05, and a minimum combined mean of 5 reads were deemed to be significantly differentially expressed. The

Ensemble annotation was enriched with UniProt data (release 06.06.2014) based on Ensembl gene identifiers (Activities at the Universal Protein Resource (UniProt)). The correlation of replicate gene counts was assessed with the Spearman ranked correlation algorithm included in R 3.11 (R: A language and environment for statistical computing). Genes regulated by age (±1 log2 fold change, basemean>5, fdr<0.05) derived from mRNASeq of killifish Nfu samples were imported into DAVID (https://david.ncifcrf.gov/) to reveal top KEGG pathways affected by age.

For ChIP sequencing, around 20 mg of skeletal muscle tissue were chopped with a scalpel, harvested in 5 ml of PBS, cross-linked by 1.5% formaldehyde for 30 min at room temperature on a rotator, and quenched with 0.125 M glycine for 5 min at room temperature. After crosslinking, tissue was washed two times in cold PBS and centrifuged at 1000 g for 5 min at 4°C. The pellet was resuspended in 0.25 ml of SDS lysis buffer (50 mM Tris pH 8.0, 1% SDS, 10 mM EDTA, anti-proteases), incubated on a rotator for 30 min at 4°C, sonicated for 18 cycles on high power setting (30s ON, 30s OFF) using the Bioruptor Next Gen (Diagenode) and centrifuged at 20000 g for 10 min at 4°C. The isolated chromatin was diluted 10-fold with ChIP dilution buffer (16.7 mM Tris-HCl pH 8.0, 0.01% SDS, 1.1 % Triton X-100, 1.2 mM EDTA, 167 mM NaCl) (1/10 was kept as input) and incubated with 4 µg of antibody overnight at 4°C on a rotator. Protein G-conjugated magnetic beads (Dynal, Thermo Fisher Scientific) were saturated with PBS/1% BSA overnight at 4°C. Next day, samples were incubated with saturated beads for two hours at 4°C on a rotator, and subsequently washed with 1 ml of cold Low salt buffer (20 mM Tris-HCl pH 8.0, 0.1 % SDS, 1% Triton X-100, 2 mM EDTA, 150 mM NaCl), 1 ml of cold High salt buffer (20 mM Tris-HCl pH 8.0, 0.1 % SDS, 1% Triton X-100, 2 mM EDTA, 500 mM NaCl), 1 ml of cold LiCl buffer (10 mM Tris-HCl pH 8.0, 1% DOC, 250 mM LiCl, 1 mM EDTA, 1% NP-40), and twice with 1 ml of cold TE buffer (10 mM Tris-HCl pH 8.0, 1 mM EDTA). The immunoprecipitated chromatin was eluted with 200 µl of Elution buffer (10 mM Tris-HCl pH 8.0, 1 mM EDTA, 1% SDS, 150 mM NaCl, 5mM DTT) for 30 min at room temperature on a rotator, and decross-linked at 65°C overnight. The decross-linked DNA was purified using QiaQuick PCR Purification Kit (Qiagen) according to the manufacture's instruction. The following antibodies were used: rabbit anti-H3K9ac (ab4441, Abcam), rabbit anti-H3K27me3 (abe44, Millipore), rabbit anti-IgG (Millipore). The purified ChIP DNA was end-repaired, dA-tailed, and adaptor-ligated using the NEBNext® DNA Library Prep Master Mix Set for Illumina (NEB) following the manufacturer's instructions. The size of the library was checked using Fragment Analyzer (Agilent) and the library was sequenced on the NextSeq500 platform (illumina). Fastq files quality check was performed with FastQC (v0.11.5). Fastq files mapping to Nfu genome (Nfu_20150522; http://nfingb.leibniz-fli.de) was performed using Bowtie (v1.1.2) with --best --strata -m 1 parameter. Duplicate reads were removed using a custom script. For peak calling, macs14 (v1.4.2) was used with --nolambda parameter and 1e-3 as p-value cutoffs. The significant peaks have been used as the reference for calculation of read per million (RPM) for each sample by using a custom script.

Sequencing data sets will be available on the public repository GEO upon publication.

### *2.6 Western Blot*

Western blotting was performed by standard procedures after tissue lysis in Laemmli buffer. Nitrocellulose blotted membranes were probed with the following antibodies: H3K27me (Abcam, ab6002), H3K9me3 (Abcam, ab8898), H4K20me3 (Abcam, ab9053), H3K4me3 (Abcam, ab8580), H3 (cell signalling), PCNA (GeneTex, GTX124496), γH2AX (Genetex, GTX127343) and α-Tubulin (Cell Signalling, 3873S). Development was performed by Odyssey CLX reader (LI-COR). Densitometry analysis was performed using LI-COR software. Signal intensity from three independent Western blots loaded with lysates derived from different individuals was used for densitometry calculations normalized to young samples.

### *2.7 Histology and Morphometric Analysis*

Immunofluorescence and immunohistochemistry analyses were carried out according standard procedures. H3K27me3 (Abcam, ab6002), H3K9Ac (Abcam, ab4441) and HP1α (Bioss, 3825R) were

used according manufacturer's instructions, and nuclei were counterstained with DAPI or TOPRO-3 solution. Sudan Black B staining was performed as described in [33]; no counterstaining with Fast Red was performed. Immunofluorescence was analyzed using a Leica TCS SP8 confocal microscope. Immunohistochemistry was analyzed using a Motic AE2000 light microscope (Motic Electric Group Co.).

### *2.8 Statistical analysis*

Statistical analyses were performed using GraphPad Prism 6 software. Sample sizes (n) were reported in the corresponding figure legend. No statistical method was used to predetermine sample size. Investigators performing sequencing analysis were blinded during the experiment. All values were presented as mean ± the standard error of the mean (s.e.m.) of at least three independent experiments, unless otherwise indicated. Statistical analyses were performed using non-parametric student's t-test (unpaired Kolmogorov-Smirnov test) when the comparison has been done between two groups and non-parametric 1-way ANOVA (unpaired Kruskal-Wallis test) for more than 2 groups. For all statistical analysis, a value of $p \leq 0.05$ was deemed statistically significant.

### *2.9 Ethics statement*

All experiments were performed in accordance with relevant guidelines and regulations. Animals were bred and kept in FLI´s fish facility according to §11 of German Animal Welfare Act. The protocols of animal maintenance were approved by the local authority in the State of Thuringia (Veterinaer- und Lebensmittelueberwachungsamt) with license number J-SHK-2684-04-08/11 (before August 2017) and J-003798 (since August 2017). Sacrifice and organ harvesting was performed according to §4(3) of German Animal Welfare Act.

## 3. Results

### *3.1. Chromatin landscape discriminates among young, adult and old Nfu.*

There is, at present, an apparent lack of information regarding epigenetic modifications and sarcopenia. Moreover, very little is known about the chromatin landscape of *Nfu* skeletal muscle and how it changes during aging. Here, experiments, aimed at exploring the chromatin landscape characterizing young, adult and old *Nfu* skeletal muscle samples, were performed on the tails of histones H3 and H4. Several characterizing modifications were identified. Specifically, in old skeletal muscle tissue, a significant increase in H3K27me3, H3K9me3 and H4 K 20 tri-methylation (H4K20me3) was observed (Figure 1a). Typically, these modifications are associated with a closed chromatin structure, heterochromatin, less accessible to transcription factors ultimately leading to gene repression. To explore further how chromatin landscape might change during aging, we extended our evaluations to histone marks for open chromatin. In aged *Nfu* skeletal muscle, western blot analysis revealed a decrease in H3K9ac and H4K16ac signals (Figure 1a). Confocal microscopy (CM) confirmed the increase in H3K27me3 (Figure 1b) and the reduction of H3K9ac (Figure 1c) in old *Nfu* skeletal muscle compared to young. Moreover, in old *Nfu* skeletal muscle tissue, CM analysis of heterochromatin protein 1 alpha (HP1α), which is an additional marker of closed chromatin, provided evidence of its co-localization with H3K27me3 (Figure 1d), suggesting further that old animal epigenome presents a predominant closed conformation. These evidences prompted us to investigate the global state of DNA methylation. Interestingly, we found that with age a gradual accumulation of 5-methyl cytosine (5mC) occurs in *Nfu* skeletal muscle tissue (Figure 1e). Similar results were obtained in satellite cells isolated from young and old *Nfu* skeletal muscle tissue (Figure S1a-b).

Taken together, these observations show that in aged *Nfu* skeletal muscle chromatin becomes more condensed and possibly less transcriptionally accessible.

Peer-reviewed version available at Cells 2019, 8, 1169; doi:10.3390/cells8101169



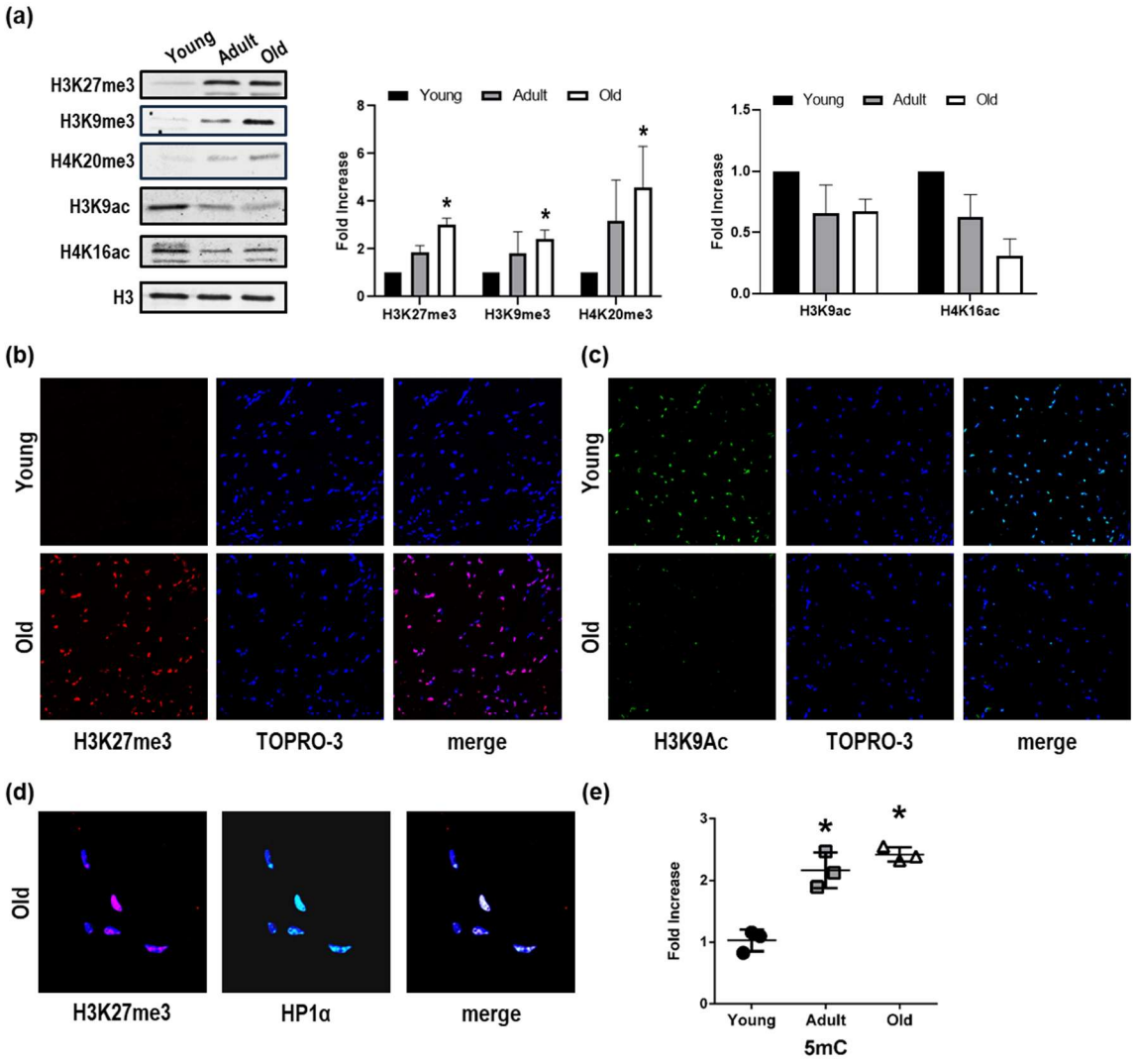


**Figure 1. Repressive histone mark accumulation and activating histone mark decrease in *Nfu* skeletal muscle tissue with age.** (**a**) Left panel: representative Western blot analysis of H3K27me3, H3K9me3, H4K20me3, H3K9ac and H4K16ac expression in young, adult and old *Nfu* muscle tissue. Total histone 3 (H3) was used as loading control. Right panel: Related densitometry analysis of H3K27me3, H3K9me3, H4K20me3, H3K9ac and H4K16ac expression in muscle tissue (n=4). *p<0.05 vs young. (**b**) Representative confocal microscopy images of H3K27me3 (red) in young (upper panel) and old (lower panel) *Nfu* skeletal muscle tissue. Nuclei were counterstained with TOPRO-3 (blue). Magnification 40x. (n=5). (**c**) Representative confocal microscopy images of H3K9Ac (green) in young (upper panel) and old (lower panel) Nfu skeletal muscle tissue; nuclei were counterstained with TOPRO-3 (blue). Magnification 40x. (n=5). (**d**) Representative confocal microscopy images of H3K27me3 (red, left panel) and heterochromatin protein 1α (HP1α, green, middle panel) in old *Nfu* skeletal muscle tissue. Merged fluorescence images are shown in the right panel (merge). Nuclei were counterstained with TOPRO-3 (blue). Magnification 40x. (n=5). (**e**) Whole skeletal muscle global DNA quantification of 5-methylcitosine (5mC) in young (black circles), adult (gray squares) and old (white triangles) *Nfu* skeletal muscle tissue expressed as fold-change versus young (n=3). *p<0.05 vs young.

*3.2 Epigenetic enzymes responsible of chromatin condensation are differentially expressed among young, adult and old Nfu.*

In association with the observed histone code modifications, the expression of a number of relevant epigenetic enzymes responsible of heterochromatin was examined. Polycomb repressive complex 2 (PRC2) is a complex with histone methyltransferase activity, which primarily leads to H3K27me3 accumulation. The mRNA levels of the three PRC2 subunits, namely ezh1, ezh2 and eed,

Peer-reviewed version available at Cells 2019, 8, 1169; doi:10.3390/cells8101169



increased in skeletal muscle tissue of old *Nfu* compared to young animals (Figure 2a). In parallel, the mRNA level of PRC1 members showed a similar trend (Figure 2b). To further characterize epigenetic enzymes involved in histone methylation, we evaluated the mRNA expression of the lysine demethylases (kdm), the enzymes involved in the removal of methyl group from lysine residues. Interestingly, compared to youngsters, mRNA levels of kdm6a and kdm6b were significantly reduced in adult *Nfu* muscle tissue, however no further changes could be detected in older animals (Figure 2c).

These findings suggest that increased levels of methylated histones might be the result of a coordinated activity between the mRNA increase of PRC members and the reduction in gene expression of lysine demethylases.

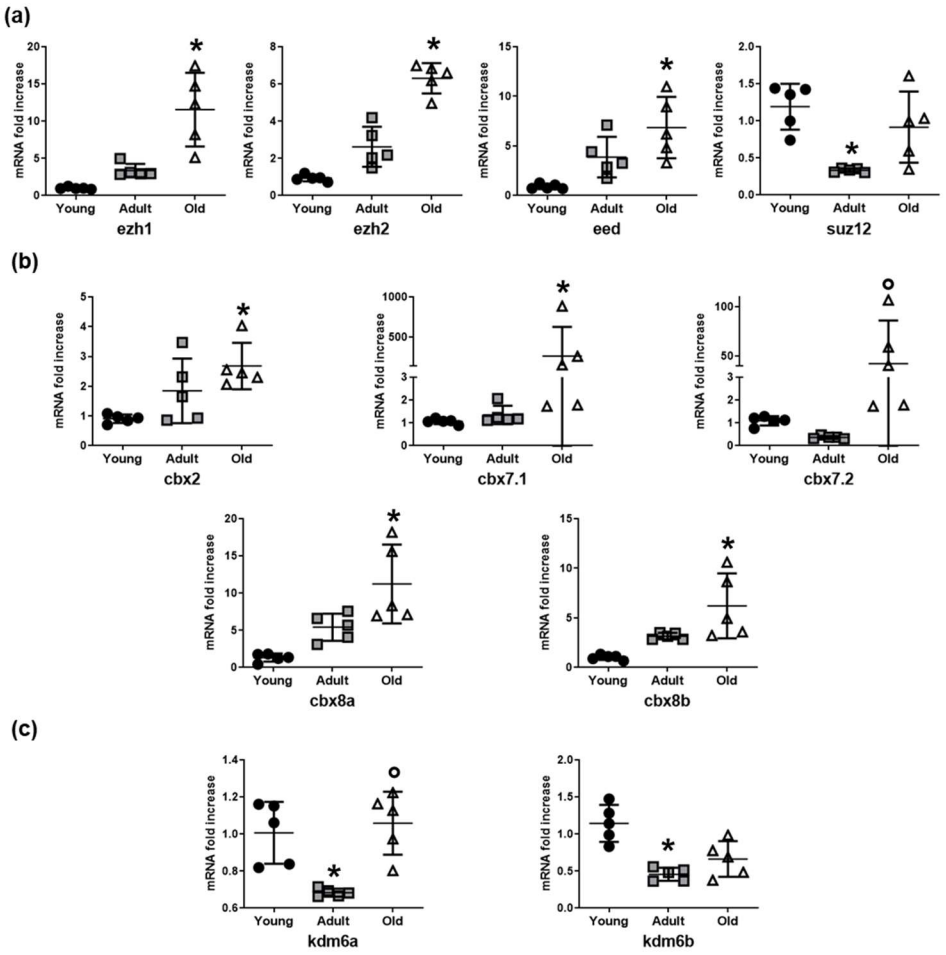


**Figure 2. Histone methylation enzyme expression increases in *Nfu* muscle tissue with age.** (***a***) qRT-PCR analysis of ezh1, ezh2, eed and suz12, polycomb repressive complex 2 (PRC2) subunits in young (black circles), adult (gray squares) and old (white triangles) *Nfu* muscle tissue expressed as fold increase versus young samples (n=5) *p<0.05 vs young. (***b***) qRT-PCR analysis of cbx2, cbx7.1, cbx7.2, cbx8a, cbx8b, a selection of polycomb repressive complex 1 (PCR1) mRNAs in young, adult and old *Nfu* muscle tissue expressed as fold increase versus young samples. (n=5). *p<0.05 vs young; °<p0.05 vs adult. (**c**) qRT-PCR analysis of lysine demethylases kdm6a and kdm6b mRNAs in young, adult and old *Nfu* muscle tissue expressed as fold increase versus young samples (n=5). *p<0.05 vs young; °<p0.05 vs adult.

*3.3 RNA sequencing of Nfu skeletal muscle tissue shows age-specific expression pattern.*

To gain insight on the aged-associated alterations in the transcriptomic of *Nfu*, young, adult and old skeletal muscle tissue transcriptomes have been explored by RNA sequencing. Specifically, 5008 differentially expressed genes (DEGs) were found analyzing *Nfu* at different ages.

After pairwise comparison of young/adult, young/old, and adult/old, 4271, 3074, and 453 genes, respectively, were found differentially expressed at more than ±1 log2 fold change (base-mean ≥5, FDR ≤0.05).

Based on multiple testing adjusted p-value criteria, the 50 most significant differentially expressed genes (DEGs) of each pair (young/adult, young/old, adult/old) were selected resulting in 122 different DEGs (Table S1). DESeq normalized counts of the selected sequences were averaged per condition and depicted as a heatmap by using a hierarchical clustering generated by Pearson correlation of the z-score (Figure 3a). The result revealed that the aging process determined important changes in the *Nfu* skeletal muscle transcriptome. Further, the partially overlapping DEGs among the experimental contrasts were utilized to identify age-specific regulated genes, and a Venn diagram was created to group RNAs into up- and down-regulated genes (Figure 3b). We identified 1063 genes down-regulated and 1138 up-regulated in adult compared to young (Figure 3b-c). The comparison of old/young alone identified 403 down-regulated and 480 up-regulated genes (Figure 3b-c). To assign a putative role to these aging-associated genes, KEGG pathway analysis was performed on significantly down- or up-regulated genes (Figure 3d). The interconnections among down-regulated genes indicated that these belong to molecular pathways associated with cell cycle progression and DNA repair. In parallel, the most up-regulated genes were enriched in gene function associated with inflammation and metabolism, with a focus on glycolysis (Figure 3d). This finding is typical of senescent cells and often co-occurs with DNA damage and the dysregulation of other aging-dependent pathways.

Altogether, these results suggest that similar to mammalians, in *Nfu* the progression of aging leads to chromatin condensation predominantly associated with regions transcribing for genes associated with proliferation and DNA repair.

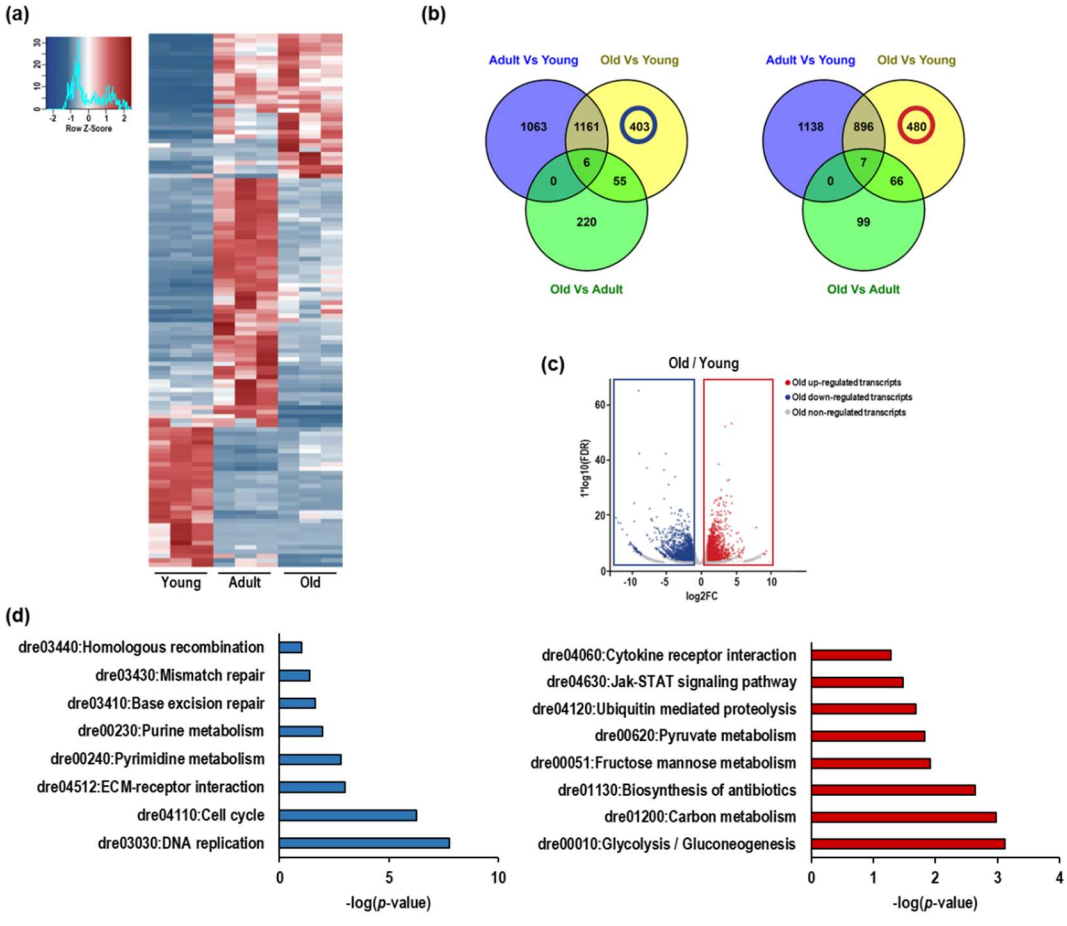

**Figure 3. The expression of DNA repair and cell cycle genes decline in *Nfu* skeletal muscle with age as expression of inflammation and glycolysis genes increase.** (**a**) Heatmap showing the 50 most significant differentially regulated genes in young, adult, old *Nfu* skeletal muscle identified by total RNA sequencing (n=3 each group). Red and blue represent over- and under-expressed genes, respectively. (**b**) Left panel: Venn diagram depicting the distribution of unique or common down regulated genes among young, adult or old *Nfu* skeletal muscle tissue at different age. Right panel: Venn diagram depicting the distribution of unique or common up-regulated genes among young, adult and old *Nfu* muscle. (**c**) Volcano plot of differentially regulated genes expressed in old *Nfu* skeletal muscle compared to young *Nfu* skeletal muscle at a multiple testing corrected p-value ≤0.05. (**d**) Left panel: KEGG pathway over-representation analysis of unique down-regulated genes between young and old *Nfu* muscle tissue (405 genes), blue bar graph. Right panel: KEGG pathway analysis of unique up-regulated genes between young and old *Nfu* muscle tissue (473 genes), red bar graph.

*3.4 H3K27me3 and H3K9ac show opposite regulation and role during aging.*

To better define the role of the observed aging-dependent histone modification alterations on DEGs we performed a chromatin immunoprecipitation-sequencing (ChIPSeq) experiment for H3K27me3 and H3K9ac enriched regions in the skeletal muscle of young and old *Nfu*. In aged animals, ChIP performed with the H3K27me3 or the H3K9ac antibody showed an accumulation of H3K27me3-enriched regions (Figure S2a). After sequencing, we mapped the reads on the *Nfu* genome and a correlation analysis of the mapped reads revealed that H3K27me3 samples separately clustered from H3K9ac samples (Figure S2b). As expected, H3K27me3 ChIP-seq was enriched on the repetitive elements and promoters of low expressed genes with a broad distribution around the transcriptional start site (TSS). Conversely, H3K9ac signals were more abundant on the promoters of expressed genes exhibiting a sharper distribution profile around TSS (Figure S2c-e). Large genomic views of the mapped reads confirmed the different distribution anticipated by ChIP-seq reads. These findings are complementary and support the whole experiment accuracy (Figure S2f). To understand whether these two epigenetic modifications correlate with the transcriptional alterations observed during aging (Figure 3), we calculated the ratio between H3K27me3 and H3K9ac signal in a subset of DEGs in old versus young *Nfu*. Except few cases (e.g. Dnmt3a), most of the down-regulated genes showed an aging-dependent increase of H3K27me3 and a relative decrease of the H3K9ac signal on their promoters. On the contrary, up-regulated genes showed an aging-dependent decrease of H3K27me3 and a relative increase of the H3K9ac signal (Figure 4a and Figure S2g). The old/young signal ratio of H3K27me3 ChIP-seq is significantly inversely correlated (Pearson = -0.57) with respect to the H3K9ac ratio indicating that these two histone modifications could have an opposite perhaps synergic role during aging (Figure 4b). Genomic views of the ChIP-seq mapped reads confirmed the opposite loss and gain of these two histone modifications in specific epigenomic regions (highlighted in yellow) and particularly around TSS (Figure 4c-d).

The results confirm the association between aging and condensed chromatin in *Nfu* skeletal muscle.

Peer-reviewed version available at Cells 2019, 8, 1169; doi:10.3390/cells8101169



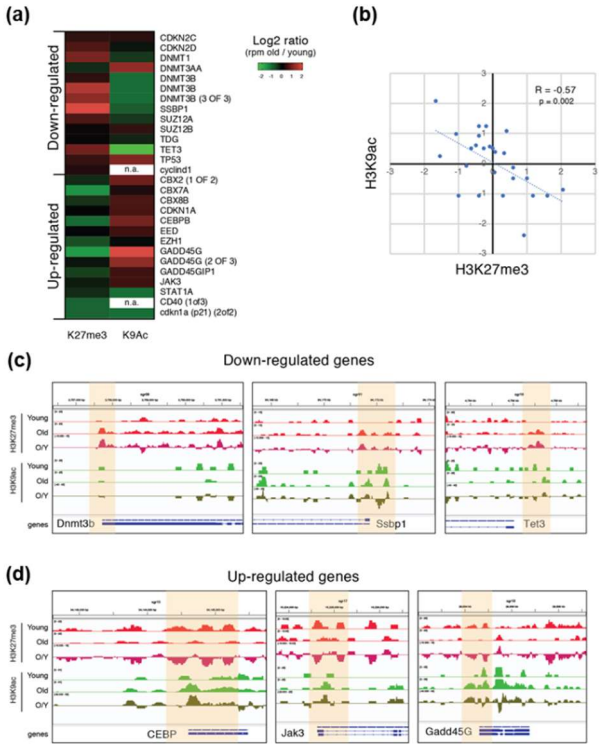


**Figure 4. ChIP-seq reveals differential roles of H3K27me3 and H3K9ac in skeletal muscle tissue.** (**a**) Heatmap showing the log2 fold change (old/young) of H3K27me3 and H3K9ac signal intensity (RPM) of some of the differentially expressed genes during aging (also see Figure S3G). RPM= Read Per Million. (**b**) Log2 fold change (old/young) of H3K27me3 (x axis) and H3K9ac (y axis) signal intensity (RPM). R and p-value is calculated using Pearson correlation. (**c** and **d**) Genomic view of the ChIP-seq mapped reads for some differentially expressed genes which is down-regulated (**c**) or up-regulated (**d**) during aging.

*3.5 Impairment of cell cycle, differentiation and DNA repair mechanics in old Nfu skeletal muscle tissue.*

The skeletal muscle tissue of old *Nfu* was further characterized by western blot and qRT-PCR to assess the expression of genes involved in cell cycle, differentiation and DNA repair. The mRNA expression of cyclin B1, fundamental for the transition through mitosis, and of cyclin D1, driving G1/S transition, were found decreased in old *Nfu* skeletal muscle tissue (Figure 5a). Consistently, the expression of proliferating cell nuclear antigen (PCNA), important for DNA replication and chromatin remodeling, was reduced in old *Nfu* muscle tissue both at mRNA and protein level (Figure 5b). Intriguingly, the decrease of markers associated to proliferation was paralleled by a reduction of the muscle-specific transcription factor, myogenin-g (Myog), which coordinates skeletal muscle development and repair (Figure 5c). Moreover, in agreement with RNA-seq analysis showing an impairment of genes involved in DNA repair, we observed a reduction in the mRNA level of the growth arrest and DNA-damage-inducible protein (gadd45γ) responsible of cellular stress response (Figure 5d). In other systems, low levels of gadd45γ have been associated with several types of tumors [34,35]. To further explore the status of DNA damage accumulation in old *Nfu* skeletal muscle, we analyzed the levels of γH2AX a marker of double-strand DNA breaks, which contributes to nucleosome formation, chromatin remodeling and DNA repair [36]. As expected, we found γH2AX enriched in old *Nfu* skeletal muscle (Figure 5e). Similar results were found in satellite cells isolated from old *Nfu* muscle tissue (Figure S1c-d).

These evidences support the bioinformatics analysis of our sequencing data set performed on *Nfu* skeletal muscle tissue during aging.

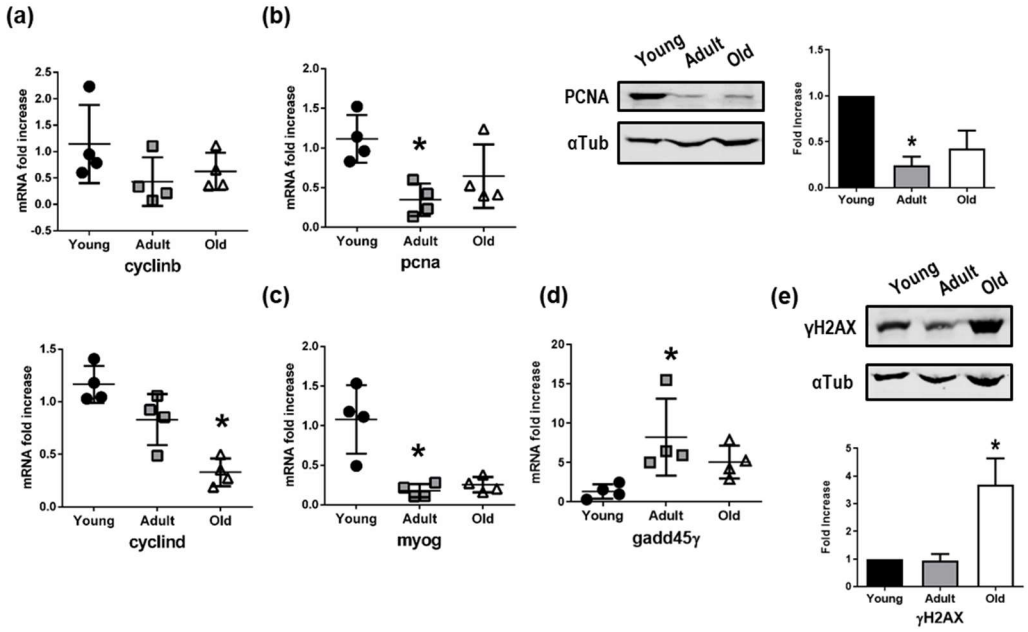


**Figure 5. Validation of mRNA sequencing.** (**a**) qRT-PCR analysis of cyclin B and cyclin D in young (black circles), adult (gray squares) and old (white triangles) *Nfu* muscle tissue expressed as fold increase versus young samples (n=4). *p<0.05 vs. young. (**b**) Left panel: qRT-PCR of the proliferating antigen (pcna), markers of cell cycle progression and proliferation. Middle panel: representative Western blot analysis of PCNA protein levels in young, adult and old *Nfu* muscle tissue. In each condition, α-tubulin (αTub) was used as loading control. Right panel: related densitometry analysis of PCNA protein levels (n=3); signal was normalized to young samples (black bars). Adult samples depicted with gray bar, old samples with white bars. *p<0.05 vs. young. (**c**) RT-PCR analysis of myogenin (myog), the transcriptional activator of muscle differentiation in young (black circles), adult (gray squares) and old (white triangles) *Nfu* muscle tissue. (n=4). *p<0.05 vs. young. (**d**) RT-PCR analysis of growth and DNA damage inducible 45γ (gadd45γ) mRNAs in young (black circles), adult (gray squares) and old (white triangles) *Nfu* skeletal muscle tissue (n=4). (**e**) Upper panel: representative Western blot analysis of γ histone 2AX (γH2AX), a marker of DNA damage, in young, adult and old *Nfu* muscle tissue. α-tubulin (αTub) was used as loading control. Lower panel: related densitometry analysis of γH2AX in muscle tissue (n=3).

### *3.6 Up-regulation of inflammation and senescence in old Nfu skeletal muscle tissue.*

Since the pairwise comparison between old and young *Nfu* skeletal muscle tissue pointed out an increase in genes involved in inflammation response, we analyzed the expression of a series of genes actively participating to immune and inflammation response. Specifically, we found an increase in the mRNA levels of the following genes: CCAAT/enhancer-binding protein beta (Cebpb), a transcription factor regulating the expression of immune and inflammatory response related genes [37]; janus kinase 3 (Jak3), coupled to cytokine receptors and responsible for their signaling transmission [38]; and pentraxin-related protein 3a (Ptx3a), a molecule released from dendritic cells, fibroblasts and endothelial cells in response to primary inflammation stimuli [39] (Figure 6a). Interestingly, a sustained inflammatory response represents a hallmark of senescence. For this reason, we investigated the degree of senescence in old *Nfu* skeletal muscle tissue. Specifically, the histological staining for Lipofuscin aggregations, detected by Sudan black b (SBB), showed evident signs of senescence in old *Nfu* skeletal muscle (Figure 6b, see black arrows), paralleled by an increase in the mRNA levels of p21, the cyclin dependent kinase inhibitor 1, a well-known senescence marker (Figure 6c). Similar results were obtained analyzing the satellite cells isolated from *Nfu* skeletal muscle for β-galactosidase (β-gal) and p21 mRNA level (Figure S1e-f). Moreover, the increased signs of senescence and the metabolic unbalance towards glycolysis extrapolated from the RNA-seq bioinformatics prompted us to analyze the *Nfu* mitochondrial function. Indeed, senescent cells accumulate dysfunctional mitochondria, characterized by decreased oxidative phosphorylation

Peer-reviewed version available at Cells 2019, 8, 1169; doi:10.3390/cells8101169



efficiency, which leads to a higher production of reactive oxygen species contributing to DNA damage accumulation [40]. In this context, a reduction in mitochondrial copy number in old *Nfu* skeletal muscle tissue (Figure 6d) was paralleled by a decreased expression of mitochondrial polymerase γ (Polγ), mitochondrial transcription factor A (Tfam) and mitochondrial single-stranded DNA-binding protein (Ssbp) (Figure 6e).

Altogether, these results indicate that aged *Nfu* skeletal muscle is characterized by an increased inflammatory response associated with senescence and mitochondrial dysfunction.

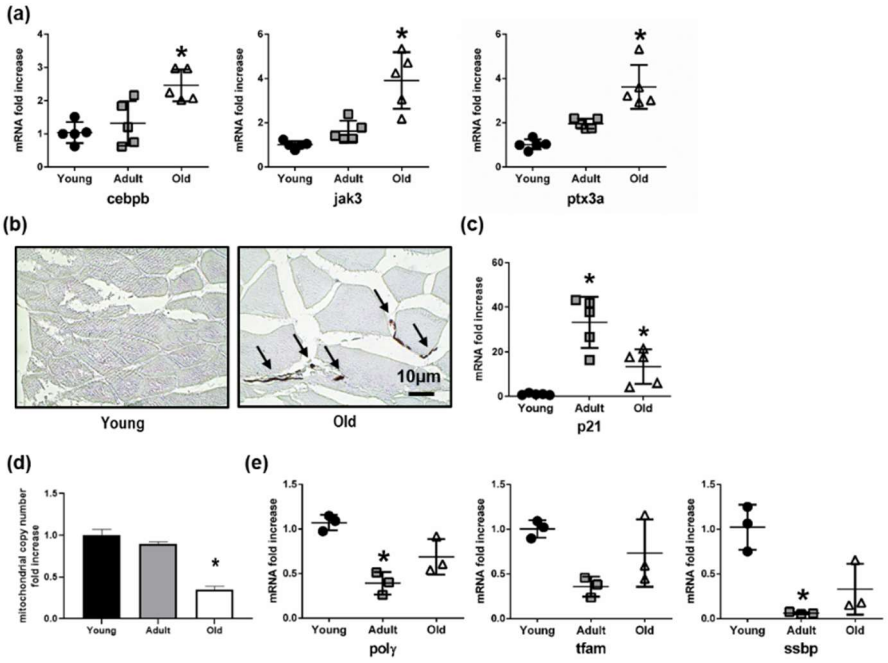


**Figure 6. Senescence increases as mitochondrial number declines in the aging *Nfu* skeletal muscle.** (**a**) Validation of sequencing results via RT-PCR analysis of mRNAs related to inflammatory signaling: CCAAT/enhancer binding protein beta (cebpb), janus kinase 3 (jak3), pentraxin 3a (ptx3a), in young (black circles), adult (gray squares) and old (white triangles) (n=5). *p<0.05 vs young. (**b**) Representative light microscopic pictures from young (right) and old (left) *Nfu* muscle stained with Sudan Black B. Accumulation of staining in the old muscle is indicated with black arrows. Calibration bar = 10µm. 40x magnification. (**c**) RT-PCR analysis of p21 mRNAs in young (black circles), adult (gray squares) and old (white triangles) *Nfu* skeletal muscle tissue (n=5). *p<0.05 vs young. (**d**) RT-PCR analysis of mitochondrial content number in young, adult and old in *Nfu* muscle tissue expressed as fold increase versus young samples (n=4). *p<0.05 vs young. (**e**) qRT-PCR analysis of mitochondrial polymerase gamma (polγ), mitochondrial transcription factor (tfam) and mitochondrial single-stranded DNA binding protein (ssbp) in young, adult and old *Nfu* muscle tissue expressed as fold increase versus young samples (n=3 at each age). *p<0.05 vs young.

## 4. Discussion

The epigenetic changes occurring during aging of *Nfu* skeletal muscle are poorly characterized. In the present study, we investigated changes of histone modifications and gene expression occurring upon age in the skeletal muscle of the turquoise killifish *Nfu*. Intriguingly, in aged *Nfu* skeletal muscle tissue, we observed a progressive increase of histone marks associated with heterochromatin (H3K27me3, H3K9me3 and H4K20me3), paralleled by a decrease in histone marks associated with euchromatin (H3K9ac and H4K16ac). The ChIP-seq analysis for H3K27me3 and H3K9ac pointed out aging-dependent gene promoters epigenetically regulated: down-regulated genes showed an enrichment of H3K27me3 associates with a relative decrease of H3K9ac, whereas up-regulated genes reported a reduction of H3K27me3 in favor of increased levels of H3K9ac, suggesting for an opposite perhaps coordinated role of these two histone modifications during aging. Similar results were

obtained in cells isolated from young and old *Nfu* skeletal muscle tissue suggesting this model as a potentially relevant *in vitro* system for the screening of senolytic and senomorphic compounds in an anti-aging perspective. In mammalian models of aging, conflicting observations have often been reported including the presence of decrease in global histone methylation occurring with age while the same modification was accumulating only at certain CpG islands [20,41]. Indeed, the differences between *Nfu* and the more characterized aging mammalian models may underline the presence of general mechanistic differences in epigenetic changes characterizing mammalian and fish during aging or be associated to the relatively very short lifespan of *Nfu*. More investigations, however, are necessary to elucidate this interesting aspect.

In the skeletal muscle of aged *Nfu*, gene expression analysis revealed a reduction of genes involved in cell cycle and proliferation, including cyclins and PCNA. Similarly, the low expression of genes associated with DNA damage, compared to younger animals, suggests an accumulation of DNA damage with aging. Although DNA damage repair is essential for replication, proliferation and tissue regeneration after injury, it seems impaired in old *Nfu* skeletal muscle as indicated by the accumulation of the modified γH2AX. Usually, in its natural habitat, killifish has only a short time period to grow and reproduce before the next dry season starts [42]. Possibly, this short lifespan compels *Nfu* to spend only little resources for DNA damage repair, a fundamental process for longer living species to counteract mutation and DNA damage accumulation [43]. Intriguingly, in other model organisms, genes involved in DNA damage repair have been shown to play essential roles in longevity, suggesting that genome maintenance in short-lived animals did not evolved as in long-lived species [43,44]. Insufficient DNA repair mechanisms could also explain the absence of lifespan extension in *Nfu* grown in fish tanks where food availability and lack of dry seasons represent optimal living conditions. On the other hand, *Nfu* might increase the proportion of heterochromatin with aging as a protective mechanism to prevent DNA breaks and other damages characterized by repetitive sequence silencing and transposon element inhibition [45]. In this light, several studies already showed the impact of heterochromatin on lifespan and genome integrity maintenance. In *Drosophila* heterochromatin formation contributes to longevity [46] and reduction of H4K16ac, via deletion of the Sas2 acetylase, apparently supports an increased lifespan [47]. In *C. elegans* the accumulation of H3K27me3 associates with increased lifespan and longevity, whereas high levels of H3K4me3 promotes the aging process [48,49].

Aging associated DNA damage partially depends on high levels of oxidative stress, which increase during lifespan, cell senescence and aging-associated diseases [50,51]. Oxidative stress products accumulate in old skeletal muscle impairing mitochondria function which is essential for muscle contraction and strength [52]. Interestingly, it has been shown that locomotor activity is impaired in aged *Nfu* [30]. Indeed, old *Nfu* showed less swimming activity and mobility suggesting that sarcopenia might occur with age [30]. Sarcopenia is also associated to increased oxidative stress and decreased muscle function [53] which might partially depend on a decreased number of functional mitochondria. In this light, we observed a decline in mitochondrial copy number in old skeletal muscle tissue of *Nfu*, in agreement with previous analyses of other *Nfu* tissues [54]. Remarkably, the parallel reduction of mitochondrial proteins in *Nfu* skeletal muscle tissue could contribute to increase oxidative stress and ultimately cause DNA damage accumulation, cell cycle arrest and senescence accelerating aging. In agreement, in old *Nfu* muscle tissue, we observed an association of increased levels of H3K9me3 with progressive accumulation of senescence markers. In particular, the so-called senescence associated heterochromatin foci (SAHFs) were found enriched in regions where H3K9me3 and HP1α localized and chromatin is more condensed [14]. Consistent with an increase of senescent markers, we found the upregulation of inflammatory signaling pathways in old *Nfu* skeletal muscle tissue, which, becoming chronic, could contribute to the so-called "inflammaging" [55]. Among other signs of aging in skeletal muscle of *Nfu*, we found an up-regulation of genes involved in glycolysis, consequent of the typical metabolic switch occurring during aging [41].

Overall, the present study shed light on the epigenetic landscape of *Nfu* skeletal muscle during aging pointing out features that may contribute to explain the loss of muscle mass, the reduction of

cell proliferation, increase of inflammation, impairment of DNA repair and the reduction in mitochondrial function. Interestingly, a recent study showed similar aging-associated transcription changes in *Nfu*, *Zebrafish*, mice and humans [56]. Altogether these observations further corroborate the use of *Nfu* as a suitable animal model for investigating the physiology and pathophysiology of aging. Comparison with datasets derived from RNA-seq of other *Nfu* tissues revealed similar gene expression changes during aging. Specifically, the RNA-seq of skin, liver and brain in old *Nfu* [57] shares at least six down-regulated and 2 up-regulated KEGG pathways with our RNA-seq conducted in skeletal muscle (Figure S3a and b). Interestingly, in old *Nfu* skeletal muscle tissue, RNA-seq performed from Reichwald's group [31] on diapause stage of *Nfu* showed a transcriptome similar to that observed in the present work (Figure S3c). Further investigation is necessary to elucidate this interesting finding. However, we can speculate that during diapause the killifish embryo undergoes severe stress situations, including aridity and temperature changes, which can contribute to the establishment of a transcriptome characterized by metabolic and cellular processes shut-down similar to the one observed during aging.

The analysis of the epigenetic landscape of *Nfu* skeletal muscle during aging, performed in this study, provides an initial characterization of the epigenetic changes occurring during *Nfu* aging, which represents an interesting starting point of investigation and to study aging in a novel experimental animal model.

**Supplementary Materials:** The following are available online at www.mdpi.com/xxx/s1, Figure S1: Cells derived from *Nfu* skeletal muscle tissues resemble tissue of origin, Figure S2: Histone marks H3K27me3 and H3K9ac cluster at the transcription start sites, Figure S3: Common mRNA expression profiles in different types of Nfu tissues during aging and during diapause indicate global trends, Table S1: Top 50 regulated genes (±1 log2 FC; base-mean ≥5, FDR ≤0.05) in each group depicted in Fig. 4A.

**Author Contributions:** Conceptualization, Francesco Spallotta and Carlo Gaetano; Data curation, Chiara Cencioni and Johanna Heid; Formal analysis, Anna Keprelova, Seyed Mohammad Mahdi Rasa, Carsten Kuenne, Stefan Guenther and Francesco Neri; Funding acquisition, Francesco Spallotta and Carlo Gaetano; Investigation, Chiara Cencioni, Johanna Heid and Francesco Spallotta; Methodology, Anna Keprelova, Seyed Mohammad Mahdi Rasa and Stefan Guenther; Resources, Mario Baumgart and Alessandro Cellerino; Software, Carsten Kuenne; Supervision, Francesco Neri, Francesco Spallotta and Carlo Gaetano; Writing – original draft, Chiara Cencioni; Writing – review & editing, Francesco Neri, Francesco Spallotta and Carlo Gaetano..

**Funding:** The present study was supported by: LOEWE Cell & Gene Therapy Center (LOEWE-CGT) Goethe University Frankfurt and by Deutsche Forschungsgemeinschaft Program SFB834 "Endothelial Signaling and Vascular Repair", Project B11 grants to CG. CG is supported by "Ricerca Corrente" Italian Ministry of Health. FS was funded by the DFG (German Research Foundation) Excellence Cluster Cardio Pulmonary System, August Scheidel-Stiftung and Amandus und Barbara Pauli Stiftung 2016.

**Conflicts of Interest:** The authors declare no conflict of interest.

## References


1. Cencioni, C.; Spallotta, F.; Martelli, F.; Valente, S.; Mai, A.; Zeiher, A.M.; Gaetano, C. Oxidative stress and epigenetic regulation in ageing and age-related diseases. *Int J Mol Sci* **2013**, *14*, 17643-17663, doi:10.3390/ijms140917643.
2. Booth, L.N.; Brunet, A. The Aging Epigenome. *Mol Cell* **2016**, *62*, 728-744, doi:10.1016/j.molcel.2016.05.013.
3. Brunet, A.; Berger, S.L. Epigenetics of aging and aging-related disease. *J Gerontol A Biol Sci Med Sci* **2014**, *69 Suppl 1*, S17-20, doi:10.1093/gerona/glu042.
4. Zenin, A.; Tsepilov, Y.; Sharapov, S.; Getmantsev, E.; Menshikov, L.I.; Fedichev, P.O.; Aulchenko, Y. Identification of 12 genetic loci associated with human healthspan. *Commun Biol* **2019**, *2*, 41, doi:10.1038/s42003-019-0290-0.
5. Benayoun, B.A.; Pollina, E.A.; Brunet, A. Epigenetic regulation of ageing: linking environmental inputs to genomic stability. *Nat Rev Mol Cell Biol* **2015**, *16*, 593-610, doi:10.1038/nrm4048.
6. Tieland, M.; Trouwborst, I.; Clark, B.C. Skeletal muscle performance and ageing. *J Cachexia Sarcopenia Muscle* **2018**, *9*, 3-19, doi:10.1002/jcsm.12238.
7. Fuggle, N.; Shaw, S.; Dennison, E.; Cooper, C. Sarcopenia. *Best Pract Res Clin Rheumatol* **2017**, *31*, 218-242, doi:10.1016/j.berh.2017.11.007.
8. McCormick, R.; Vasilaki, A. Age-related changes in skeletal muscle: changes to life-style as a therapy. *Biogerontology* **2018**, *19*, 519-536, doi:10.1007/s10522-018-9775-3.
9. Larsson, L.; Degens, H.; Li, M.; Salviati, L.; Lee, Y.I.; Thompson, W.; Kirkland, J.L.; Sandri, M. Sarcopenia: Aging-Related Loss of Muscle Mass and Function. *Physiol Rev* **2019**, *99*, 427-511, doi:10.1152/physrev.00061.2017.
10. Allis, C.D.; Jenuwein, T. The molecular hallmarks of epigenetic control. *Nat Rev Genet* **2016**, *17*, 487-500, doi:10.1038/nrg.2016.59.
11. Jung, M.; Pfeifer, G.P. Aging and DNA methylation. *BMC Biol* **2015**, *13*, 7, doi:10.1186/s12915-015-0118-4.
12. Horvath, S. DNA methylation age of human tissues and cell types. *Genome Biol* **2013**, *14*, R115, doi:10.1186/gb-2013-14-10-r115.
13. Cedar, H.; Bergman, Y. Linking DNA methylation and histone modification: patterns and paradigms. *Nat Rev Genet* **2009**, *10*, 295-304, doi:10.1038/nrg2540.
14. Chandra, T.; Narita, M. High-order chromatin structure and the epigenome in SAHFs. *Nucleus* **2013**, *4*, 23-28, doi:10.4161/nucl.23189.
15. Hernandez-Segura, A.; Nehme, J.; Demaria, M. Hallmarks of Cellular Senescence. *Trends Cell Biol* **2018**, *28*, 436-453, doi:10.1016/j.tcb.2018.02.001.
16. Aird, K.M.; Zhang, R. Detection of senescence-associated heterochromatin foci (SAHF). *Methods Mol Biol* **2013**, *965*, 185-196, doi:10.1007/978-1-62703-239-1_12.
17. Roth, S.Y.; Denu, J.M.; Allis, C.D. Histone acetyltransferases. *Annu Rev Biochem* **2001**, *70*, 81-120, doi:10.1146/annurev.biochem.70.1.81.
18. Gates, L.A.; Shi, J.; Rohira, A.D.; Feng, Q.; Zhu, B.; Bedford, M.T.; Sagum, C.A.; Jung, S.Y.; Qin, J.; Tsai, M.J., et al. Acetylation on histone H3 lysine 9 mediates a switch from transcription initiation to elongation. *J Biol Chem* **2017**, *292*, 14456-14472, doi:10.1074/jbc.M117.802074.

19. Taylor, G.C.; Eskeland, R.; Hekimoglu-Balkan, B.; Pradeepa, M.M.; Bickmore, W.A. H4K16 acetylation marks active genes and enhancers of embryonic stem cells, but does not alter chromatin compaction. *Genome Res* **2013**, *23*, 2053-2065, doi:10.1101/gr.155028.113.

20. Weidner, C.I.; Wagner, W. The epigenetic tracks of aging. *Biol Chem* **2014**, *395*, 1307-1314, doi:10.1515/hsz-2014-0180.

21. O'Sullivan, R.J.; Karlseder, J. The great unravelling: chromatin as a modulator of the aging process. *Trends Biochem Sci* **2012**, *37*, 466-476, doi:10.1016/j.tibs.2012.08.001.

22. Aranda, S.; Mas, G.; Di Croce, L. Regulation of gene transcription by Polycomb proteins. *Sci Adv* **2015**, *1*, e1500737, doi:10.1126/sciadv.1500737.

23. Cellerino, A.; Valenzano, D.R.; Reichard, M. From the bush to the bench: the annual Nothobranchius fishes as a new model system in biology. *Biol Rev Camb Philos Soc* **2016**, *91*, 511-533, doi:10.1111/brv.12183.

24. Genade, T.; Benedetti, M.; Terzibasi, E.; Roncaglia, P.; Valenzano, D.R.; Cattaneo, A.; Cellerino, A. Annual fishes of the genus Nothobranchius as a model system for aging research. *Aging Cell* **2005**, *4*, 223-233, doi:10.1111/j.1474-9726.2005.00165.x.

25. Kim, Y.; Nam, H.G.; Valenzano, D.R. The short-lived African turquoise killifish: an emerging experimental model for ageing. *Dis Model Mech* **2016**, *9*, 115-129, doi:10.1242/dmm.023226.

26. Terzibasi, E.; Valenzano, D.R.; Benedetti, M.; Roncaglia, P.; Cattaneo, A.; Domenici, L.; Cellerino, A. Large differences in aging phenotype between strains of the short-lived annual fish Nothobranchius furzeri. *PLoS One* **2008**, *3*, e3866, doi:10.1371/journal.pone.0003866.

27. Di Cicco, E.; Tozzini, E.T.; Rossi, G.; Cellerino, A. The short-lived annual fish Nothobranchius furzeri shows a typical teleost aging process reinforced by high incidence of age-dependent neoplasias. *Exp Gerontol* **2011**, *46*, 249-256, doi:10.1016/j.exger.2010.10.011.

28. Hartmann, N.; Reichwald, K.; Lechel, A.; Graf, M.; Kirschner, J.; Dorn, A.; Terzibasi, E.; Wellner, J.; Platzer, M.; Rudolph, K.L., et al. Telomeres shorten while Tert expression increases during ageing of the short-lived fish Nothobranchius furzeri. *Mech Ageing Dev* **2009**, *130*, 290-296, doi:10.1016/j.mad.2009.01.003.

29. Harel, I.; Benayoun, B.A.; Machado, B.; Singh, P.P.; Hu, C.K.; Pech, M.F.; Valenzano, D.R.; Zhang, E.; Sharp, S.C.; Artandi, S.E., et al. A platform for rapid exploration of aging and diseases in a naturally short-lived vertebrate. *Cell* **2015**, *160*, 1013-1026, doi:10.1016/j.cell.2015.01.038.

30. Valenzano, D.R.; Terzibasi, E.; Cattaneo, A.; Domenici, L.; Cellerino, A. Temperature affects longevity and age-related locomotor and cognitive decay in the short-lived fish Nothobranchius furzeri. *Aging Cell* **2006**, *5*, 275-278, doi:10.1111/j.1474-9726.2006.00212.x.

31. Reichwald, K.; Petzold, A.; Koch, P.; Downie, B.R.; Hartmann, N.; Pietsch, S.; Baumgart, M.; Chalopin, D.; Felder, M.; Bens, M., et al. Insights into Sex Chromosome Evolution and Aging from the Genome of a Short-Lived Fish. *Cell* **2015**, *163*, 1527-1538, doi:10.1016/j.cell.2015.10.071.

32. Valenzano, D.R.; Benayoun, B.A.; Singh, P.P.; Zhang, E.; Etter, P.D.; Hu, C.K.; Clement-Ziza, M.; Willemsen, D.; Cui, R.; Harel, I., et al. The African Turquoise Killifish Genome Provides Insights into Evolution and Genetic Architecture of Lifespan. *Cell* **2015**, *163*, 1539-1554, doi:10.1016/j.cell.2015.11.008.

33. Evangelou, K.; Gorgoulis, V.G. Sudan Black B, The Specific Histochemical Stain for Lipofuscin: A Novel Method to Detect Senescent Cells. *Methods Mol Biol* **2017**, *1534*, 111-119, doi:10.1007/978-1-4939-6670-7_10.

34. Garcia, V.; Garcia, J.M.; Pena, C.; Silva, J.; Dominguez, G.; Rodriguez, R.; Maximiano, C.; Espinosa, R.; Espana, P.; Bonilla, F. The GADD45, ZBRK1 and BRCA1 pathway: quantitative analysis of mRNA expression in colon carcinomas. *J Pathol* **2005**, *206*, 92-99, doi:10.1002/path.1751.
35. Higashi, H.; Vallbohmer, D.; Warnecke-Eberz, U.; Hokita, S.; Xi, H.; Brabender, J.; Metzger, R.; Baldus, S.E.; Natsugoe, S.; Aikou, T., et al. Down-regulation of Gadd45 expression is associated with tumor differentiation in non-small cell lung cancer. *Anticancer Res* **2006**, *26*, 2143-2147.
36. Kuo, L.J.; Yang, L.X. Gamma-H2AX - a novel biomarker for DNA double-strand breaks. *In Vivo* **2008**, *22*, 305-309.
37. Rahman, S.M.; Janssen, R.C.; Choudhury, M.; Baquero, K.C.; Aikens, R.M.; de la Houssaye, B.A.; Friedman, J.E. CCAAT/enhancer-binding protein beta (C/EBPbeta) expression regulates dietary-induced inflammation in macrophages and adipose tissue in mice. *J Biol Chem* **2012**, *287*, 34349-34360, doi:10.1074/jbc.M112.410613.
38. Wang, H.; Brown, J.; Gao, S.; Liang, S.; Jotwani, R.; Zhou, H.; Suttles, J.; Scott, D.A.; Lamont, R.J. The role of JAK-3 in regulating TLR-mediated inflammatory cytokine production in innate immune cells. *J Immunol* **2013**, *191*, 1164-1174, doi:10.4049/jimmunol.1203084.
39. Bottazzi, B.; Inforzato, A.; Messa, M.; Barbagallo, M.; Magrini, E.; Garlanda, C.; Mantovani, A. The pentraxins PTX3 and SAP in innate immunity, regulation of inflammation and tissue remodelling. *J Hepatol* **2016**, *64*, 1416-1427, doi:10.1016/j.jhep.2016.02.029.
40. Fang, E.F.; Scheibye-Knudsen, M.; Chua, K.F.; Mattson, M.P.; Croteau, D.L.; Bohr, V.A. Nuclear DNA damage signalling to mitochondria in ageing. *Nat Rev Mol Cell Biol* **2016**, *17*, 308-321, doi:10.1038/nrm.2016.14.
41. Lopez-Otin, C.; Blasco, M.A.; Partridge, L.; Serrano, M.; Kroemer, G. The hallmarks of aging. *Cell* **2013**, *153*, 1194-1217, doi:10.1016/j.cell.2013.05.039.
42. Blazek, R.; Polacik, M.; Reichard, M. Rapid growth, early maturation and short generation time in African annual fishes. *Evodevo* **2013**, *4*, 24, doi:10.1186/2041-9139-4-24.
43. Tian, X.; Firsanov, D.; Zhang, Z.; Cheng, Y.; Luo, L.; Tombline, G.; Tan, R.; Simon, M.; Henderson, S.; Steffan, J., et al. SIRT6 Is Responsible for More Efficient DNA Double-Strand Break Repair in Long-Lived Species. *Cell* **2019**, *177*, 622-638 e622, doi:10.1016/j.cell.2019.03.043.
44. Lidzbarsky, G.; Gutman, D.; Shekhidem, H.A.; Sharvit, L.; Atzmon, G. Genomic Instabilities, Cellular Senescence, and Aging: In Vitro, In Vivo and Aging-Like Human Syndromes. *Front Med (Lausanne)* **2018**, *5*, 104, doi:10.3389/fmed.2018.00104.
45. Janssen, A.; Colmenares, S.U.; Karpen, G.H. Heterochromatin: Guardian of the Genome. *Annu Rev Cell Dev Biol* **2018**, *34*, 265-288, doi:10.1146/annurev-cellbio-100617-062653.
46. Larson, K.; Yan, S.J.; Tsurumi, A.; Liu, J.; Zhou, J.; Gaur, K.; Guo, D.; Eickbush, T.H.; Li, W.X. Heterochromatin formation promotes longevity and represses ribosomal RNA synthesis. *PLoS Genet* **2012**, *8*, e1002473, doi:10.1371/journal.pgen.1002473.
47. Kozak, M.L.; Chavez, A.; Dang, W.; Berger, S.L.; Ashok, A.; Guo, X.; Johnson, F.B. Inactivation of the Sas2 histone acetyltransferase delays senescence driven by telomere dysfunction. *EMBO J* **2010**, *29*, 158-170, doi:10.1038/emboj.2009.314.
48. Han, S.; Brunet, A. Histone methylation makes its mark on longevity. *Trends Cell Biol* **2012**, *22*, 42-49, doi:10.1016/j.tcb.2011.11.001.

694 49. Maures, T.J.; Greer, E.L.; Hauswirth, A.G.; Brunet, A. The H3K27 demethylase UTX-1 regulates C.
695 elegans lifespan in a germline-independent, insulin-dependent manner. *Aging Cell* **2011**, *10*, 980-990,
696 doi:10.1111/j.1474-9726.2011.00738.x.
697 50. Bu, H.; Wedel, S.; Cavinato, M.; Jansen-Durr, P. MicroRNA Regulation of Oxidative Stress-Induced
698 Cellular Senescence. *Oxid Med Cell Longev* **2017**, *2017*, 2398696, doi:10.1155/2017/2398696.
699 51. Xie, Y.; Chen, Y. microRNAs: Emerging Targets Regulating Oxidative Stress in the Models of
700 Parkinson's Disease. *Front Neurosci* **2016**, *10*, 298, doi:10.3389/fnins.2016.00298.
701 52. Romanello, V.; Sandri, M. Mitochondrial Quality Control and Muscle Mass Maintenance. *Front Physiol*
702 **2015**, *6*, 422, doi:10.3389/fphys.2015.00422.
703 53. Powers, S.K. Can antioxidants protect against disuse muscle atrophy? *Sports Med* **2014**, *44 Suppl 2*, S155-
704 165, doi:10.1007/s40279-014-0255-x.
705 54. Hartmann, N.; Reichwald, K.; Wittig, I.; Drose, S.; Schmeisser, S.; Luck, C.; Hahn, C.; Graf, M.;
706 Gausmann, U.; Terzibasi, E., et al. Mitochondrial DNA copy number and function decrease with age in
707 the short-lived fish Nothobranchius furzeri. *Aging Cell* **2011**, *10*, 824-831, doi:10.1111/j.1474-
708 9726.2011.00723.x.
709 55. Franceschi, C.; Campisi, J. Chronic inflammation (inflammaging) and its potential contribution to age-
710 associated diseases. *J Gerontol A Biol Sci Med Sci* **2014**, *69 Suppl 1*, S4-9, doi:10.1093/gerona/glu057.
711 56. Aramillo Irizar, P.; Schauble, S.; Esser, D.; Groth, M.; Frahm, C.; Priebe, S.; Baumgart, M.; Hartmann,
712 N.; Marthandan, S.; Menzel, U., et al. Transcriptomic alterations during ageing reflect the shift from
713 cancer to degenerative diseases in the elderly. *Nat Commun* **2018**, *9*, 327, doi:10.1038/s41467-017-02395-
714 2.
715 57. Baumgart, M.; Groth, M.; Priebe, S.; Savino, A.; Testa, G.; Dix, A.; Ripa, R.; Spallotta, F.; Gaetano, C.;
716 Ori, M., et al. RNA-seq of the aging brain in the short-lived fish N. furzeri - conserved pathways and
717 novel genes associated with neurogenesis. *Aging Cell* **2014**, *13*, 965-974, doi:10.1111/acel.12257.
718